Solvent Effects on Internal Rotational Barriers in Furfural. NMR Measurements and ab-Initio Molecular Orbital Methods Using Continuum Models

Alex D. Bain* and Paul Hazendonk

Department of Chemistry, McMaster University, Hamilton, Ontario, Canada L8S 4M1

Received: May 6, 1997; In Final Form: June 30, 1997[⊗]

Modern experimental and theoretical methods for determining solvent effects on internal rotational barriers in small molecules are compared. The barrier to rotation of the aldehyde group in furfural dissolved in toluene, acetone, and methanol is used as a test case. Ab-initio molecular orbital methods such as self consistent reaction field (SCRF) calculations, performed with the Onsager and isodensity surface polarized continuum (IPC) model, predict an increase in barrier with increasing solvent dielectric constant, ϵ. A combination of three nuclear magnetic resonance experiments are used to obtain rate data over 6 orders of magnitude representing an approximately 150 K temperature range. Activation parameters were obtained with errors less than 1 kJ/mol and 6 J/(mol K) for $\Delta H^{\ddagger}$ and $\Delta S^{\ddagger}$, respectively. In acetone and toluene large $\Delta S^{\ddagger}$ values of −26 and 20 J/(mol K) were found, along with a ΔS° of 10 J/(mol K) in both solvents. In methanol no appreciable values for $\Delta S^{\ddagger}$ and ΔS° were measured. The $\Delta H^{\ddagger}$ for toluene, acetone, and methanol are 48.6, 40.2, and 46.4 kJ/mol, respectively, which do not obey a simple relationship with ϵ. This indicates that the solvent effect is likely more complex than just the effect of a solvent reaction field. The large $\Delta S^{\ddagger}$ values support this and also imply that equating $\Delta G^{\ddagger}$ and $\Delta H^{\ddagger}$ is not always justified, even for aprotic solvents. The behavior of these three barriers and their corresponding $\Delta S^{\ddagger}$ are discussed in terms of direct solvent−solute interactions.

Introduction

Rotations of chemical bonds in molecules are seldom "free". In other words there is always some barrier to rotation, which can furthermore depend on solvent. Studies into solvent effects on these processes are primarily concerned with measurement or theoretical predictions. Measurements are achieved mainly by nuclear magnetic resonance (NMR), microwave, and infrared (IR) spectroscopies. Barriers are computed using molecular orbital calculations of the solute in the presence of the reaction field due to the solvent. The main aim of this study is to compare the most recent methods of measurement with prediction, on a sample system.

Usually NMR rate measurements are made with line shape fitting procedures.[1−9] Due to limits on the temperature range over which rate measurements can be made, barriers are often reported as $\Delta G^{\ddagger}$.[8,10−14] To compare these barriers with calculations (which give $\Delta H^{\ddagger}$), $\Delta S^{\ddagger}$ is often assumed to be zero.[8,15] This assumption is not unreasonable since these are unimolecular processes. However, there are cases where $\Delta S^{\ddagger}$ is observed to be significantly nonzero.[16,17]

Calculations of internal rotational barriers in solvent usually include continuum models,[18−21] which compute the electrostatic contribution to the free energy of solvation. The total energy is just a combination of the free energy of solvation with the gas phase energy. To make the model more complete, the electrostatic solvation energy is often accompanied by contributions from cavitation and dispersion energies.[20,22] Recently, the electrostatic interaction has been incorporated into the Fock operator of the solute, including it in the self-consistent cycles which optimize the electron density. This allows the solute to be polarized by the solvent field.[23−25] Second derivatives of this self consistent reaction field energy, with respect to the nuclear coordinates, are now readily determined, making transition state searches and frequency calculations possible.[26,27] With these developments, barriers in liquid phase are as readily obtained as in gas phase, with some additional computational effort. It should be stressed however that these methodologies do not account for direct solute−solvent interactions.

In order to obtain good experimental values of $\Delta H^{\ddagger}$ and $\Delta S^{\ddagger}$, rate measurements are needed over as wide a range as possible. Recently this laboratory developed a technique that employs three complementary NMR experiments.[5,7,28−32] These, when combined, are capable of generating rate data over 6 orders of magnitude, corresponding to temperature ranges of ca. 150 °C. Measurements made on furfural in acetone revealed that the $\Delta H^{\ddagger}$ was much smaller than previously seen in polar solvents and a large negative $\Delta S^{\ddagger}$ was observed.[29] $\Delta G^{\ddagger}(298)$ was in line with the previous experimental and theoretical studies. Consequently ignoring the entropy of activation is not always justified and equating $\Delta G^{\ddagger}$ with $\Delta H^{\ddagger}$ can be misleading.

This study will compare barriers calculated by recently developed computational methodologies with those measured by the most accurate NMR methods for furfural in toluene, acetone, and methanol. Measurements will be carried out with the three NMR experiment techniques, and computations will employ self consistent reaction field (SCRF) methods using the Onsager[23−25] and Tomasi's isodensity surface polarized continuum (IPC) models.[33,34] The importance of considering $\Delta S^{\ddagger}$ will be discussed.

Methodology

Rate Measurements. The most common way of measuring rates by NMR is with line shape methods. These rates are only accurate when the line shape in question is broad,[8,28,29] which occurs when the line width is dominated by the contribution from exchange and other line-broadening factors are small in comparison. In the extreme ranges of measurement, both when the rates are slow and fast, the lines are narrow and other line-broadening factors become significant.[35] As a result the rates

* Author to whom correspondence should be addressed.

[⊗] Abstract published in *Advance ACS Abstracts,* August 15, 1997.

S1089-5639(97)01520-X CCC: $14.00

Figure 1. Isomerization of furfural from its O,O-cis to its O,O-trans form.

may be overestimated in the slow regime and underestimated in the fast exchange regimes, giving rise to systematic errors in $\Delta H^{\ddagger}$ and $\Delta S^{\ddagger}$. Therefore it is necessary to make additional measurements of slow and fast rates which are independent of these broadening effects.

In the slow exchange regime, where the conformer lifetime is on the same order of magnitude as the spin−lattice relaxation times of the observed nuclei, the rate can be measured using the selective inversion experiment.[31,32,36,37] The line corresponding to one site is inverted selectively, and the relaxation of both lines is observed. The exchange rate can be extracted by fitting the data to the set of differential equations that describe the relaxation and exchange behavior.

In the fast exchange regime T_2 is measured independently of the magnetic field inhomogeneities using the offset saturation experiment.[30] The decoupler is tuned near the spectral line, which is irradiated for a period long enough to establish a steady state. After a short delay an FID is acquired. A plot of the partially saturated line intensity as a function of offset frequency exhibits a dip at resonance, whose width at half-depth is $\gamma B_2(T_1/T_2)^{1/2}$.[38] With independent measurements of T_1 and γB_2, T_2 can be determined, which in turn is directly related to the rate.[3]

Solvent Calculations. The barrier to interconversion between the O,O-cis and O,O-trans forms of furfural (Figure 1) will be computed in gas and solvent phase up to the MP2/6-31G** level. With both the gas phase and SCRF calculations, the transition state geometries will be determined at saddle points in the energy surface with respect to the reaction coordinates. The SCRF techniques will employ the Onsager and the IPC models. Both these models assume the solute is in a cavity of a given shape which is surrounded by a polarizable continuous medium with dielectric constant ϵ.[18−21,23−25,39] The solute electron density polarizes the medium, causing the medium to impose an inhomogeneous electric field onto the solvent, leading to a net stabilization. The reaction field can polarize the solute, altering the electric field it produces, which in turn changes the reaction field itself, and so on, leading to higher order corrections to the solvation energy. The two solvent models differ mainly in the way the reaction field is modeled.

The Onsager model assumes a perturbation to the Hamiltonian of the isolated solute molecule based on the interaction energy between the molecular dipole ($\boldsymbol{\mu}$) and the reaction field ($\boldsymbol{R}$), $H_1 = -\boldsymbol{\mu}\cdot\boldsymbol{R}$.[23] The reaction field is related to the molecular dipole and the cavity radius (a_0) as in eq 1. The cavity radius is usually

$$\vec{\boldsymbol{R}} = g\vec{\boldsymbol{\mu}}; \quad g = \frac{2(\epsilon - 1)}{(2\epsilon + 1)a_0^{\,3}} \tag{1}$$

based on the molar volume of the solute. The interaction energy term can be included directly into the Fock matrix as in (2),

$$F_{\lambda\sigma} = F^{\circ}_{\lambda\sigma} - g\vec{\boldsymbol{\mu}}\langle\phi_\lambda|\vec{\boldsymbol{\mu}}|\phi_\sigma\rangle \tag{2}$$

where ϕ_λ and ϕ_σ are basis functions.[23] In SCRF calculations the molecular dipole moment is not computed as an expectation value but rather as a derivative of the solute energy with respect to a uniform electric field.[23] The total energy including the contribution due to solvent polarization is given in (3),

$$E = \langle\Psi|H_0|\Psi\rangle - (1/2)\vec{\boldsymbol{\mu}}\cdot\vec{\boldsymbol{R}} \tag{3}$$

where Ψ is the full wave function. First- and second-order energy derivatives with respect to nuclear coordinates are easily obtained for geometry optimizations and transition state searches.[26]

The implementation of the Tomasi model considered in this study is based on the apparent surface charge approach.[19] Initially the electric field, E_s, from the solute charge density induces a dipole density distribution $P(r)$ in the continuum.[21]

$$\vec{\boldsymbol{P}}(r) = (1 - \epsilon)\vec{\boldsymbol{E}}(r) = (1 - \epsilon)(\vec{\boldsymbol{E}}_{\mathbf{s}}(r) + \vec{\boldsymbol{E}}_{\mathbf{p}}(r)) \tag{4}$$

In this equation, $\boldsymbol{E}(r)$ is the total electric field at r including the contribution from the dipoles themselves. From Gauss' law, the potential from the solvent dipole field can be described as arising from a charge density on the surface of the cavity by (5),

$$\sigma(r_s) = -\frac{(\epsilon - 1)}{4\pi\epsilon}[\vec{\boldsymbol{E}}_{\mathbf{0}}(R_s) + \vec{\boldsymbol{E}}_{\bar{\mathbf{p}}}(r_s)]\cdot\vec{\boldsymbol{n}}(r_s) \tag{5}$$

where $n(r_s)$ is the vector normal to the cavity surface at a point on the surface r_s.[20] The potential from this surface charge distribution is included in the solute Hamiltonian, H_0, for self consistent isodensity polarized continuum calculations. In eq 6 the Hamiltonian is made up of three parts: the isolated solute molecule Hamiltonian, H_0, the contribution of the solute electron density, and the contribution of the nuclei to the reaction field potential.[33]

$$H = H_0 - \sum_i \oint \frac{\sigma_{\bar{p}}(r_s)\,\mathrm{d}r_s}{|r_i - r_s|} + \sum_n Z_n \oint \frac{\sigma_{\bar{p}}(r_s)\,\mathrm{d}r_s}{|R_n - r_s|} \tag{6}$$

The Onsager method is simpler than the Tomasi method and is thus not expected to be as accurate. It restricts the electrostatic energy to the dipole−induced dipole contribution and ignores higher order terms.[19] Due to its simplicity, its main advantage is that computations can be performed quickly. Its main disadvantage is that its conventional implementation is restricted to using spherical and ellipsoidal cavity shapes. The results are also dependent on cavity dimensions, often making interpretation of the results arbitrary.[23] The Tomasi model includes the higher order electrostatic terms, so it should give more accurate electrostatic contributions to the solvation energy.[19] Its main disadvantage is that it requires much more computational effort than the Onsager method, needing as much as 50% additional CPU time.[33] Its main advantage is its ability to use arbitrary cavity shapes, reflecting the actual structure of the solute. Despite the different advantages and disadvantages of both methods, both performed equally well in studies into the solvent effect on the gauche−trans ratios of 1,2-dichloroethane.[23,33]

A Brief Overview of the Literature on Furfural. Experiments on furfural have focused mainly on the relative conformer stabilities.[40−63] After some initial confusion,[60] the O,O-trans form was seen to predominate in the gas phase,[58] and a transition occurs to the O,O-cis in media with ϵ greater than 5.[22,40,43,46,57,63] Theoretical studies employing both classical reaction field and SCRF methodologies reproduce this trend closely.[22,23,57,62,63] The gas phase energy difference is 6.3 kJ/mol.[63]

Measurements of the barrier in furfural are rare. To date, barriers are known only in gas phase and a few solvents. Microwave experiments by Mönnig and infrared measurements by Miller gave gas phase barriers of 34 and 25 kJ/mol,

TABLE 1: Summary of Temperature, Rate, and Equilibrium Constant Data for Furfural in Toluene, Acetone, and Methanol, As Obtained from the NMR Analyses

	toluene			acetone			methanol		
T^a	$k_{c-t}{}^b$	K^c	E[d]	k_{c-t}	K	E	k_{c-t}	K	E
177				0.20	0.10	si			
180							0.18	0.17	si
182				0.44	0.10	si			
185	0.88	0.24	si				0.63	0.18	si
190	1.89	0.26	si	1.60	0.11	si	1.13	0.19	si
195				3.25	0.13	ls			
200	10.0	0.30	ls						
205	23.0	0.31	ls	11.3	0.15	ls	16.0	0.21	ls
210	40.0	0.33	ls	30.0	0.20	ls	28.6	0.22	ls
215	80.0	0.35	ls	46.8	0.28	ls	51.8	0.23	ls
220	135	0.37	ls				88.5	0.24	ls
225	225	0.39	ls				150	0.24	ls
230	415	0.41	ls	110	0.30	T	258	0.25	ls
235	715	0.42	ls	260	0.31	T	417	0.26	ls
240	1200	0.44	ls	403	0.32	T	630	0.27	ls
245	1980	0.46	ls				922	0.28	ls
250	3150	0.48	ls	819	0.33	T	2217	0.28	T
260	11 300	0.52	T				5150	0.29	T
262.5				2680	0.35	T			
275				7290	0.37	T			
282.5				11 400	0.38	T			
292.5				17 800	0.39	T			
297	237 000	0.65	T						
300				31 100	0.40	T			
305	388 000	0.68	T						
310				43 800	0.41	T	173 000	0.36	T
317.5				61 400	0.42	T			

[a] All temperatures are given in Kelvin. [b] All rates are cis to trans rates. [c] Equilibrium constants were calculated from integration values of the cis and trans aldehyde proton signal in the low-temperature spectra. At room temperature the equilibrium constants were taken from the literature. The intermediate values were obtained by extrapolation with the van't Hoff isochore. [d] The columns with heading E indicate with which experiment the rate was measured (si, selective inversion; ls, line shape; and T, the offset saturation experiment).

respectively.[59] In solution they are 44 kJ/mol for dimethyl ether and 46 kJ/mol for neat solution.[63] Studies predicting this barrier in solvent are restricted to Abraham and Siverns,[63] Birnstock,[22] Benassi,[62] and In-Suk Han[64] who found that the barriers increased with increasing dielectric constant, as was seen experimentally. The results of Abraham and Han agree closely with experiment. Bennassi's analysis, which includes contributions from cavitation and dispersion energies, overemphasizes this effect tremendously. Birstock's approach, similar to that of Bennasi's, predicts a barrier around 50 kJ/mol in tetrachloromethane,[22] which is large compared to 44 kJ/mol measured in dimethyl ether. The more recent study by Han uses single-point Onsager SCRF calculations with MP2/6-31+G** geometries giving barriers of 38.6 kJ/mol in gas phase and 46.8 kJ/mol in a medium with $\epsilon = 78.54$.

Results

The rate constants at various temperatures for the cis−trans process, k_{c-t}, in toluene, acetone, and methanol are given in Table 1 along with their equilibrium constants. The equilibrium constants were obtained by extrapolating low-temperature values to room temperature values using the van't Hoff isochore. In toluene and acetone significant entropy differences ($\Delta S°$) between the cis and trans forms were observed. The equilibrium constants at low temperature were determined by integration of the spectral lines, and those at room temperature were given by Bertran and others.[44,57,63] The Eyring plots are shown in Figure 2. The relative error in rate constants, at 95% confidence,

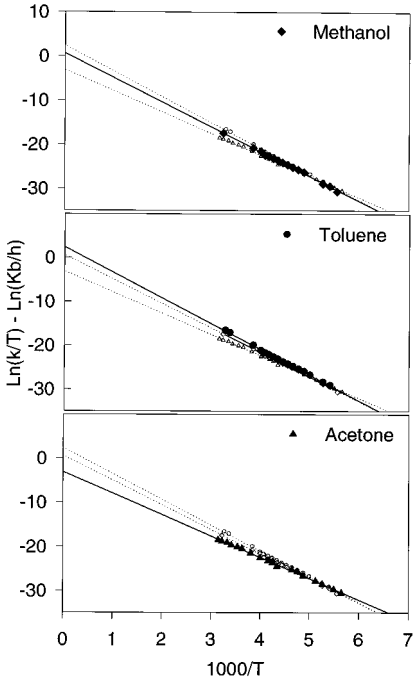

Figure 2. Eyring plots of the rate data in methanol (top, ■), toluene (middle, ●), and acetone (bottom, ▲), each with the remaining plots in the background.

TABLE 2: Activation and Equilibrium Thermodynamic Parameters of Furfural in Three Solvents, Determined by NMR Chemical Exchange Measurements

solvent	$\Delta H^{\ddagger}_{ct}$	$\Delta H°$	$\Delta S^{\ddagger}_{ct}$	$\Delta S°$	$\Delta G^{\ddagger}_{ct}$	K_{eq}
toluene	48.6[a]	4.0	20[b]	10	42.7[c]	0.64[d]
acetone	40.2	5.1	−26	10	47.8	0.45
methanol	46.4	2.6	5	0	44.9	0.33

[a] All enthalpies are given in kJ/mol. The error is taken directly from the regression error of the slope of the Eyring plot and is approximately 1 kJ/mol at the 95% confidence. [b] All Entropies are given in J/(mol K). The error, including the contribution from the uncertainty in the slope of the Eyring plot, is approximately 6 J/(mol K) at the 95% confidence. [c] All Gibbs free energies are given in kJ/mol and are evaluated at 298 K. [d] Equilibrium constants are trans/cis and are evaluated at 298 K.

are below 10% for all three methods. The thermodynamic parameters, for both k_{c-t} and k_{t-c}, obtained from the Eyring plots are given in Table 2. Values for k_{t-c} were computed from the corresponding k_{c-t} and equilibrium constant. By moving the origin to the average 1000/T value, any covariance between the error in the slope and that of the intercept is removed.[28] The error in the $\Delta H^{\ddagger}$ was taken directly from the regression error in the slope (Δm). The error in $\Delta S^{\ddagger}$ was computed with the regression error in the intercept (Δy) and slope using (7),

$$8.314\sqrt{\Delta m^2 x^2 + \Delta y^2} \qquad (7)$$

where x is the average of 1000/T.

The total and relative calculated electronic energies along with the electric dipole moments of all three geometries of furfural are shown in Table 3. All relative energies are reported with respect to the energy of the O,O-trans form. The MP2/6-31G** geometries of the cis, trans, and transition forms are given in Table 4. The results from the self-consistent IPC/6-31G calculations with geometry optimization are shown in Table 5. The stabilization due to the solvent for each geometry is reported with respect to the corresponding gas phase value. The predicted barriers at the 6-31G level with geometry optimization are given in Table 6. These barriers were corrected using MP2/

TABLE 3: Energies and Dipole Moments of the Three Conformations of Furfural Obtained from Molecular Orbital Calculations

basis	property	O,O-trans	O,O-cis	transition state
STO-3G	E	−336.982 18[a]	−336.980 95	−336.972 18
	ΔE_{trans}	0[b]	3.23	26.24
	μ	1.83[c]	2.41	1.81
6-31G	E	−341.200 51	−341.196 05	−341.181 58
	ΔE_{trans}	0	11.69	49.69
	μ	3.98	5.21	3.92
6-31G**	E	−341.364 07	−341.362 02	−341.346 66
	ΔE_{trans}	0	5.38	45.71
	μ	3.50	4.32	3.21
MP2/6-31G**	E	−341.358 64	−341.356 27	−341.340 81
	ΔE_{trans}	0	6.22	46.81
	μ	3.87	4.75	3.43

[a] All total energies are given in hartrees. [b] All relative energies are given in kJ/mol. [c] All electric dipole moments given in debyes.

TABLE 4: Geometries of the Cis, Trans, and Transition Forms of Furfural as Determined by MP2/6-31G Calculations: All Geometries Were Allowed To Fully Relax; Bond Lengths Are Given in Angstroms and Angles Are Given in Degrees**

parameter	cis	trans	‡	parameter	cis	trans	‡
C1−C2	1.379	1.377	1.369	C1−C6−O7	124.6	122.9	122.5
C2−C3	1.418	1.417	1.427	C1−C6−H8	113.5	114.9	116.7
C3−C4	1.371	1.372	1.366	C1−C2−H9	125.9	125.2	126.2
C4−O5	1.360	1.361	1.368	C2−C3−H10	127.8	127.6	127.4
C1−C6	1.457	1.458	1.493	C3−C4−H11	133.4	133.6	134.0
C6−O7	1.227	1.229	1.224	C1−C2−C3−C4	0.0	0.0	−0.2
C6−H8	1.104	1.103	1.102				
C2−H9	1.078	1.077	1.077	C2−C3−C4−O5	0.0	0.0	0.0
C3−H10	1.076	1.077	1.076	C3−C2−C1−C6	180.0	180.0	181.0
C4−H11	1.076	1.076	1.075	C2−C1−C6−O7	180.0	0.0	91.7
				C2−C1−C6−H8	0.0	180.0	−88.3
C1−C2−C3	106.4	106.3	106.1	O5−C1−C2−H9	180.0	180.0	179.9
C2−C3−C4	106.0	106.4	106.4	C1−C2−C3−H10	180.0	180.0	179.6
C3−C4−O5	110.9	110.6	110.4	C2−C3−C4−H11	180.0	180.0	180.0
C2−C1−C6	131.5	133.1	133.6				

TABLE 5: Solvent Calculations with the Self Consistent Isodensity Surface Polarized Continuum Model to the 6-31G Level on the Cis, Trans, and Transitions Forms of Furfural

medium	property	O,O-cis	O,O-trans	transition state
gas	E[a]	−341.1961	−341.2005	−341.1816
toluene	E	−341.2029	−341.2057	−341.1868
	ΔE[b]	−17.87	−13.56	−13.64
acetone	E	−341.2104	−341.2108	−341.1923
	ΔE	−37.79	−27.15	−28.18
methanol	E	−341.2109	−341.2111	−341.1927
	ΔE	−39.04	−27.90	−29.08

[a] Total energies including the stabilization due to solvent. These are reported in hartrees. [b] Energies relative to gas phase. These are reported in kJ/mol.

6-31G** gas phase relative conformer stabilities and SC-IPC/6-31G stabilization energies and are seen in Table 7. Barriers from the Onsager and IPC single-point calculations at 6-31G** and MP2/6-31G** are given in Table 8. These were performed with 6-31G** and MP2/6-31G** gas phase geometries. The IPC MP2/6-31G** results are depicted in Figure 3 and are compared with measured barriers in Figure 4. Onsager SCRF calculations with geometry optimizations indicated no significant change in gas and liquid phase geometries using $\epsilon = 32.63$.

Discussion

The assignment of the O,O-cis form as the major conformer in acetone was done previously by an NOE difference experiment;[29] this was an expected result since the cis form is known to predominate in polar solvents.[22,40,43,46,57,63] Based on the five-bond coupling constant from the aldehyde proton to the proton ortho to the ring oxygen, $^5J_{H8,H11}$, the cis conformer was found to prevail in toluene and methanol as well. These couplings were both 1.08 Hz, which is in line with those measured by Dahlqvist and Forsen.[60,65]

The rates were determined over 6 orders of magnitude corresponding to a temperature range of ca. 190−310 K. Thus the errors in both the slope and the intercept of the Eyring plots are much lower than with analyses using only line shape methods. The 95% confidence limits for the entropies of activation are 6 J/(mol K) and for the corresponding enthalpies are around 1 kJ/mol.

TABLE 6: Barrier to Internal Rotation of the Aldehyde Group, E(cis) − E(trans) and Electric Dipole Moments of Furfural As Predicted by SCIPC HF/6-31G Calculations

	ΔEt‡[a]	ΔEc‡	ΔEtc	μ_{cis}[b]	μ_{trans}	$\mu_{‡}$
gas	49.96[c]	38.00	11.69	5.21	3.98	3.92
toluene	49.61	42.23	7.37	5.94	4.50	4.32
acetone	48.66	47.61	1.05	6.77	5.03	4.75
MeOH	48.52	47.97	0.55	6.82	5.06	4.77

[a] The change in energy between the transition state (‡) and the trans conformer (t) (c stands for the cis conformer). [b] Molecular dipoles computed in solvent field. All dipoles are given in debyes. [c] All relative energies are reported in kJ/mol.

TABLE 7: Internal Rotational Barrier in Furfural Predicted by Combining Gas Phase Values from MP2/6-31G Computations and Stabilization Energies from Self-Consistent IPC HF/6-31G Calculations**

	ΔEt‡[a]	ΔEc‡	ΔEtc[c]
gas	46.81[b]	40.59	6.22
toluene	46.81	44.79	2.02
acetone	45.76	50.04	−4.27
MeOH	45.49	50.30	−4.80

[a] The change in energy between the transition state (‡) and the trans conformer (t) (c stands for the cis conformer). [b] Gas phase values from MP2/6-31G** calculations. All relative energies are reported in kJ/mol. [c] Stabilization energies due to solvent taken from SCIPC HF/6-31G calculations (see Table 3).

TABLE 8: Single-Point Self-Consistent IPC and Onsager Calculations Employing Gas Phase Geometries from 6-31G and MP2/6-31G** Calculations**

	SCIPC HF/6-31G**[a]			SCIPC MP2/6-31G**[b]		
solvent	ΔEt‡	ΔEc‡	ΔEtc	ΔEt‡	ΔEc‡	ΔEtc
gas[c]	45.71[d]	40.33	−5.38	46.82[e]	40.61	−6.22
toluene	45.64	43.26	−2.38	47.13	44.31	−2.81
acetone	44.86	46.51	1.66	46.66	48.46	1.81
methanol	44.79	46.72	1.93	46.59	48.71	2.12
	Onsager HF/6-31G**[f]			Onsager MP2/6-31G**[g]		
solvent	ΔEt‡	ΔEc‡	ΔEtc	ΔEt‡	ΔEc‡	ΔEtc
gas	45.71[d]	40.33	−5.38	46.82[e]	40.61	−6.22
toluene	46.40	43.06	−3.34	49.23	46.78	−2.45
acetone	47.46	46.44	−1.02	53.29	55.35	2.06
methanol	47.54	46.67	−0.87	53.60	55.95	2.36

[a] Single-point SCRF calculations using the 6-31G** basis, HF/6-31G** gas phase geometries, and the isodensity surface polarized continuum model. [b] Single-point MP2 SCRF calculations using the 6-31G** basis, MP2/6-31G** gas phase geometries, and the isodensity surface polarized continuum model. [c] Gas phase energies at the 6-31G** level. [d] All energies are given in kJ/mol. [e] Gas phase energies at the MP2/6-31G** level. [f] Single-point SCRF calculations using the 6-31G** basis, HF/6-31G** gas phase geometries, and the Onsager model. [g] Single-point MP2 SCRF calculations using the 6-31G** basis, MP2/6-31G** gas phase geometries, and the Onsager model.

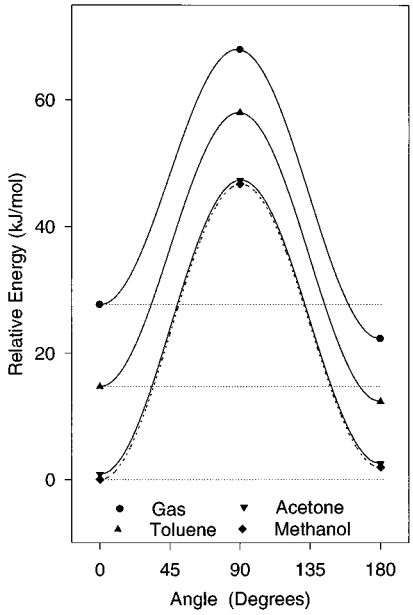

Figure 3. Barrier in three solvents and gas phase compared on an absolute scale. This depicts the stabilization due to the solvent field with respect to gas phase, given by single-point SCIPC MP2/6-31G** calculations (see Table 8). Notice differential stabilization of the cis form with respect to the trans form. The gas phase energies are from MP2/6-31G** calculations. The single-point SCIPC calculations were performed at MP2/6-31G** using MP2/6-31G** geometries. The energy of the cis conformer in methanol is set to zero.

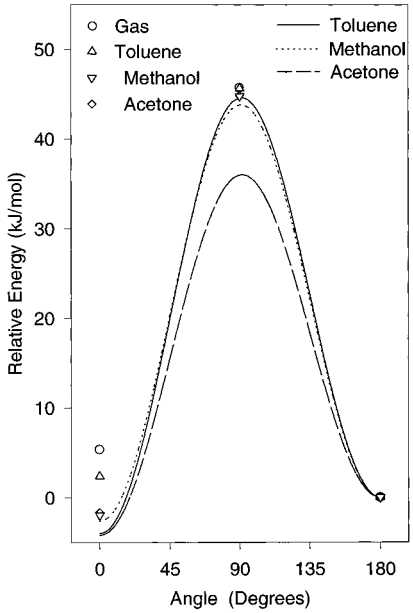

Figure 4. Schematic comparison between the experimental barriers and those determined by single SCIPC MP2/6-31G** calculations. The experimental barriers are given in Table 2, and the computed barriers are from Table 8. The experimental barriers are shown as curves, while the computational results are given as symbols.

The rate data were determined using three different trial sets of equilibrium constants, *K*, based on different methods of extrapolation with the van't Hoff isochore. The first method employs only the low-temperature *K*'s and makes no assumption about $\Delta S°$. The second method is similar to the first except that it assumes $\Delta S°$ is zero. The last method uses room temperature *K*'s from the literature,[57,63,66] based on NMR coupling constants, and those measured at low temperature. The third method gave the best fitting Eyring plots where the data sets from all three NMR experiments fell closely along a straight line (Figure 3). In the other two methods the offset saturation data did not line up as well with the two remaining data sets. Lastly, the first two methods greatly over- and underestimate the room-temperature equilibrium constants. In the third approach $\Delta S^{\ddagger}$'s and $\Delta S°$'s were the least extreme.

Having nonzero entropies is not unreasonable. The dipole moment and shape of the molecule change significantly throughout the rotational process; thus it is possible that changes occur in the steric and electrostatic interactions with local solvent molecules. These changes could affect the organization of the local solvent, giving rise to changes in entropy.

For all calculation levels but STO-3G, the gas phase cis−trans and trans−cis barriers are both overestimated by the HF calculations. At 6-31G** and MP2/6-31G** levels the cis−trans barrier is 40 kJ/mol, which is 4 kJ/mol larger than the measured values. The energy difference between the two planar forms is 5−6 kJ/mol, which is close to 6.28 kJ/mol reported previously.[58,59,63] The electronic dipole moments of the trans and cis conformers given in the literature are 3.23 and 3.97 D; the transition state dipole moment was predicted to be 2.93 D.[41,63] Both 6-31G** and MP/6-31G** overestimate them; however their relative sizes are approximately correct.

It is better to follow the behavior of the cis−trans barrier since it expected to be the most sensitive to solvent effects. Both theory and experiment have shown that the dipole moment of the cis form is much larger than the trans form, as one might expect. Thus in environments of high dielectric constant, the cis form should be the most stabilized. The trans dipole moment is approximately the same size as that of the transition state; thus the barrier from trans to cis is expected to be least sensitive to ϵ, as opposed to the cis to trans barrier, which is expected to increase significantly.

The solvent calculations predict the same trend in relative conformer stabilities and barrier heights with respect to ϵ as previous investigations.[22,23,57,62,63] For the self-consistent IPC method it was necessary to go to the 6-31G** level to obtain the correct behavior, and electron correlation was required for the Onsager SCRF approach. The self-consistent IPC calculations with the 6-31G basis did not recover the correct behavior primarily because the gas phase energy difference between the cis and trans conformer, ΔE_{ct}, is greatly overestimated. When using the MP2/6-31G** for ΔE_{ct} the stabilization of the cis with respect to the trans conformer is predicted for $\epsilon > 5$. The self-consistent IPC calculations at 6-31G** and MP2/6-31G** come closest to previous work, the barrier increases by 6−8 kJ/mol from gas to liquid phase ($\epsilon = 32.63$), and in methanol and acetone it is predicted to be at least 3 kJ/mol larger than in toluene.

The behavior of the enthalpies of activation for the cis−trans process with respect to ϵ deviates from previous observations[61,63] and predictions.[22,62−64] The value for toluene ($\epsilon = 2.38$) is 8 kJ/mol larger than in acetone ($\epsilon = 20.7$). No simple trend is observed with respect to ϵ, except that the barrier increases when going from gas to liquid phase. When considering the free energy of activation at 298 K, the relative order of toluene and acetone is reversed, which is in line with previous work. Thus the observed solvent effect is contrary to predictions made by current theoretical methods.[62−64] Since the barriers do not obey a simple relationship with ϵ, it would seem that there is more at play than just the effect of a solvent field. Consequently the reaction field methods by themselves should not be expected to account for this behavior.

The behavior of $\Delta H^{\ddagger}_{ct}$ and $\Delta S^{\ddagger}_{ct}$ can be understood more clearly if direct interactions with the solvent are considered. These interactions can be steric, electrostatic, or bonding in nature, giving rise to some type of preferred solute−solvent

structure. In toluene the large entropy of activation of +20 J/(mol K) indicates that the transition state is disordered with respect to the planar forms, which implies that there is some preferred orientation of the solvent with respect to the planar forms. Rotational processes could disrupt this solute−solvent structure, possibly increasing the enthalpy of activation due to steric interactions between the solvent and the transition state. In acetone, the transition state is ordered when compared to the planar forms, as is indicated by an entropy of activation of −26 J/(mol K). Thus there is some preferred assembly of solvent with the transitions state that is disrupted when going to the planar forms. Steric interactions between the solvent and the ring could destabilize the planar forms, decreasing the barrier.

In methanol ($\epsilon = 32.63$) there is no significant entropy of activation, indicating that there is no preferred interaction between the solute and any of the solute forms. This is not to say that there are no direct solute−solvent interactions, because they are well−known for furfural and primary alcohols.[67] The barrier in methanol is the most compatible with that determined in neat furfural[63] and agrees reasonably with SCI-PCM calculations.

Conclusions

This study has served to illustrate that large entropies of activation exist for aprotic solvents like acetone and toluene. This is by no means the first observation of entropy effects, but the combination of excellent experimental data and good calculations makes the effects particularly clear. This means that entropies of activation cannot be ignored for internal rotations and that measured enthalpies need to be reported in the literature. Approaches to modeling medium effects on these processes should allow for local interactions with the solvent.

Experimental Section

Furfural was purchased from Aldrich and was used without further purification. Samples, of approximately 5 mol %, were prepared in toluene-d_8, acetone-d_6, and methanol-d_4. These were degassed with five freeze−pump−thaw cycles and were sealed under vacuum. Tetramethylsilane was used as an internal chemical shift and line-width reference.

All ^{1}H NMR measurements were performed on a Bruker AC-300 spectrometer using a 5 mm four-nucleus probe. Temperature control was maintained to within ±0.5 °C using a BVT 2000 temperature controller and was monitored periodically by inserting a copper-constantan thermocouple in a 5 mm NMR tube into the probe.

The selective inversion experiments were carried out employing the relaxation−$\pi/2-\tau-\pi/2$−variable delay−$\pi/2$−acquisition pulse sequence. The carrier frequency was set to the resonance to be inverted, typically the major site. The delay, τ, was set to $1/(2\Delta\nu_{\mathrm{cis-trans}})$, where $\Delta\nu_{\mathrm{cis-trans}}$ is the frequency difference between the cis and trans signal, which varied with solvent from 50 Hz in acetone to 120 Hz in toluene. The variable delays, VD, were chosen from a range of 10 ms to 10 s, and the relaxation delay was typically 20 s. Line intensity measurements of this data were obtained via the XWINNMR package (Bruker) and were analyzed with CIFIT, a program developed in this lab based on the SIFIT program written by R. E. D. McClung and R. Muhandiram.[68]

Line shape analysis was performed with the MEX program. MEX simulates line shapes of exchanging systems without scalar coupling. The simulated spectra are directly imported into XWINNMR and compared with experiment using the dual display mode.

The off-resonance saturation experiments, described in previous work,[29,30] were performed using the proton homodecoupler set to high power providing a saturating field. The field strength of the decoupler was calibrated using the single-spin double-resonance experiment, with the TMS signal. The values for $\gamma B_2/2\pi$ were typically 30−40 Hz. The T_1 for the aldehyde signal ranged from 5 to 40 s with increasing temperature; consequently the irradiation periods required in the off-resonance saturation experiment ranged over 30−200 s. The preacquisition delay was set to typically $0.1T_1$ and thus ranged from 0.5 to 4 s. The free induction decays were obtained with a $\pi/2$ pulse using 6 kHz sweep widths. Decoupler frequencies were chosen with emphasis on the region near the half-height of the curve of intensity as a function of offset frequency. An average of 35 frequencies were used.

The intensities, relative to that furthest from resonance, were analyzed using DIPPER, a nonlinear least-squares fitting program. Values for T_1 and T_2 were obtained in this manner. Separate inversion recovery experiments were carried out at each temperature to obtain an independent value of T_1.

Restricted Hartree−Fock calculations were performed using Gaussian 94[69] with an IBM RS 6000 470 series computer. Optimum states of both the cis and trans conformers were computed to the MP2/6-31G** level. Transition state calculations were performed using the QST3 method of searching for saddle points in the energy surface, available in Gaussian 94. Self consistent reaction field computations were done with the Onsager and isodensity surface polarized continuum model. Both the optimum and transition geometries were determined with the SCIPC method to the 6-31G level and up to the 6-31G** level for the Onsager SCRF approach. The dielectric constants employed were 20.7, 32.63, and 2.38 for acetone, methanol, and toluene, respectively.[70] Using gas phase geometries from 6-31G** and MP2/6-31G** single-point SCRF computations, reaction field calculations were performed via both models at 6-31G** and MP/6-31G** levels. The cavity radius was 3.70 Å.[23]

Acknowledgment. We would like thank Dr. T. Schaefer for letting us use his computational facilities and G. Bernard for his help with the solvent calculations. This work was supported by the Natural Sciences and Engineering Research Council of Canada (NSERC).

References and Notes

(1) Gutowsky, H. S.; Holm, C. H. *J. Chem. Phys.* **1956**, *25*, 1228−1234.
(2) Szymanski, S.; Witanowski, M.; Gryff-Keller, A. M. *Annual Reports on NMR Spectroscopy*; Webb, G. A., Ed.; Academic Press: London, 1978; pp 227−289.
(3) Piette, L. H.; Anderson, W. A. *J. Chem. Phys.* **1959**, *30*, 899−908.
(4) Orrell, K. G.; Sik, V. *Annu. Rep. NMR Spectrosc.* **1987**, *19*, 79−173.
(5) Bain, A. D.; Duns, G. J. *J. Magn. Reson.* **1995**, *112 A*, 258−260.
(6) Binsch, G. *J. Am. Chem. Soc.* **1969**, *91*, 1304−1309.
(7) Bain, A. D.; Duns, G. J. *Can. J. Chem.* **1996**, *74*, 819−824.
(8) Kessler, H. *Angew. Chem., Int. Ed. Engl.* **1970**, *9*, 219−235.
(9) Inglefield, P. T.; Krakower, E.; Reeves, L. W.; Stewart, R. *Mol. Phys.* **1968**, *15*, 65−86.
(10) Stewart, W. E.; Siddall, T. H. *Chem. Rev.* **1970**, *70*, 517−551.
(11) Friedl, Z.; Bohm, S.; Goljer, I.; Piklerova, A.; Poorova, D.; Rickova, A.; Kovac, J. *Collect. Czech. Chem. Commun.* **1987**, *52*, 409−424.
(12) Haushalter, K. A.; Lau, J.; Roberts, J. D. *J. Am. Chem. Soc.* **1996**, *118*, 8891−8896.
(13) Turnbull, M. M.; Nelson, D. J.; Lekouses, W.; Sarnov, M. L.; Tartarini, K. A.; Huang, T. *Tetrahedron* **1990**, *46*, 6613−6622.
(14) Saurez, C.; LeMaster, C. B.; LeMaster, C. L.; Tafazzoli, M.; True, N. S. *J. Phys. Chem.* **1990**, *94*, 6679−6683.
(15) Laidler, K. J., *Chemical Kinetics*; 2nd ed.; McGraw Hill: New York, 1965.

(16) Berg, U.; Sjostrand, U. *Org. Magn. Reson.* **1978**, *11*, 555−560.
(17) Tyson, R. L.; Weil, J. A. *J. Phys. Chem.* **1990**, *94*, 3951−3958.
(18) Onsager, L. *J. Am. Chem. Soc.* **1936**, *58*, 1486−1493.
(19) Tomasi, J.; Persico, M. *Chem. Rev.* **1994**, *94*, 2027−2094.
(20) Miertus, S.; Tomasi, J. *Chem. Phys.* **1982**, *65*, 239−245.
(21) Miertus, S.; Scrocco, E.; Tomasi, J. *Chem. Phys.* **1981**, *55*, 117−129.
(22) Birnstock, F.; Hofman, H. J.; Kohler, H. J. *Theor. Chim. Acta (Berlin)* **1997**, *42*, 311−323.
(23) Wong, M. W.; Frisch, M. J.; Wiberg, K. B. *J. Am. Chem. Soc.* **1991**, *113*, 4776−4782.
(24) Wong, M. W.; Wiberg, K. B.; Frisch, M. J. *J. Am. Chem. Soc.* **1992**, *114*, 1645−1652.
(25) Wiberg, K. B.; Wong, M. W. *J. Am. Chem. Soc.* **1993**, *115*, 1078−1084.
(26) Wong, M. W.; Wiberg, K. B.; Frisch, M. J. *J. Chem. Phys.* **1991**, *95*, 8991−8998.
(27) Dillet, V.; Rinaldi, D.; Bertran, J.; Rivail, J. L. *J. Chem. Phys.* **1996**, *23*, 9437−9444.
(28) Bain, A. D.; Duns, G. J.; Ternieden, S.; Ma, J.; Werstiuk, N. H. *J. Phys. Chem.* **1994**, *98*, 7458−7463.
(29) Bain, A. D.; Duns, G. J.; Rathgeb, F.; Vanderkloet, J. *J. Phys. Chem.* **1995**, *99*, 17338−17343.
(30) Bain, A. D.; Duns, G. J. *J. Magn. Reson.* **1994**, *109A*, 56−64.
(31) Bain, A. D.; Cramer, J. A. *J. Phys. Chem.* **1993**, *97*, 2884−2887.
(32) Bain, A. D.; Cramer, J. A. *J. Magn. Reson.* **1993**, *103 A*, 217−222.
(33) Wiberg, K. B.; Keith, T. A.; Frisch, M. J.; Murko, M. *J. Phys. Chem.* **1995**, *99*, 9072−9079.
(34) Wiberg, K. B.; Rablem, P. R.; Rush, D. J.; Keith, T. A. *J. Am. Chem. Soc.* **1995**, *117*, 4261−4270.
(35) Drakenberg, T.; Carter, R. E. *Org. Magn. Reson.* **1975**, *7*, 307−308.
(36) Forsen, S.; Hoffman, R. A. *J. Chem. Phys.* **1963**, *39*, 2892−2901.
(37) Hoffman, R. E.; Forsen, S. *Prog. Nucl. Magn. Reson. Spectrosc.* **1966**, *1*, 15−204.
(38) Tomlinson, G. *J. Magn. Reson.* **1983**, *52*, 374−385.
(39) Alagona, G.; Ghio, C.; Igual, J.; Tomasi, J. *J. Molec. Struct. (THEOCHEM)* **1990**, *204*, 253−283.
(40) Benassi, R.; Folli, U.; Schenetti, L.; Taddei, F. *Adv. Heterocycl. Chem.* **1997**, *41*, 75−186.
(41) Liegeous, C.; Barker, J. M.; Lumbroso, H. *Bull. Soc. Chim. Fr.* **1978**, *7*−8, I-329−I-332.
(42) Benassi, R.; Folli, U.; Mucci, A.; Schenetti, L.; Taddei, F. *Magn. Reson. Chem.* **1987**, *25*, 804−810.
(43) Benassi, R.; Folli, U.; Schenetti, L.; Taddei, F. *J. Chem. Soc., Perkin Trans. 2* **1988**, 1501−1507.
(44) Bertran, J. F.; Rodriguez, M. *Org. Magn. Reson.* **1974**, *6*, 525−527.
(45) Roques, B.; Combrisson, S.; Riche, C.; Pascard-Billy, C. *Tetrahedron* **1970**, *26*, 3555−3567.
(46) Chadwick, D. J. *J. Chem. Soc., Perkin Trans. 2* **1976**, 451−452.
(47) Martin, M. L.; Roze, J.-C.; Martin, G. J.; Fournari, P. *Tetrahedron Lett.* **1970**, *39*, 3407−3410.
(48) Abraham, R. J.; Chadwick, D. J.; Sancassan, F. *Tetrahedron* **1982**, *38*, 3245−3254.
(49) Roques, B.; Combrisson, S.; Wehrli, F. *Tetrahedron Lett.* **1975**, *12*, 1047−1050.
(50) Roques, B.; Fournie-Zaluski, M. C. *Org. Magn. Reson.* **1971**, *3*, 305−312.
(51) Chadwick, D. J.; Meakins, G. D.; Richards, E. E. *Tetrahedron Lett.* **1974**, *36*, 3183−3184.
(52) Caccamese, S.; Montaudo, G.; Recca, A.; Fringuelli, F.; Taticchi, A. *Tetrahedron* **1974**, *30*, 4129−4135.
(53) Chadwick, D. J.; Chambers, J. M.; Meakins, G. D.; Snowden, R. L. *J. Chem. Soc., Chem. Commun.* **1971**, 624−625.
(54) Abraham, R. J.; Chadwick, D. J.; Sancassan, F. *Tetrahedron* **1982**, *38*, 1485−1491.
(55) Barili, P. L.; Lunazzi, L.; Veracini, C. A. *Mol. Phys.* **1972**, *24*, 673−677.
(56) Montaudo, G.; Caccamese, S.; Librando, V.; Maravigna, P. *Tetrahedron* **1973**, *29*, 3915−3923.
(57) Petrongolo, C. *Chem. Phys. Lett.* **1976**, *42*, 512−516.
(58) Miller, F. A.; Fateley, W. G.; Witkowski, R. E. *Spectrochim. Acta* **1967**, *23A*, 891−908.
(59) Allen, G.; Bernstein, H. J. *Can. J. Chem.* **1955**, *33*, 1055−1061.
(60) Dahlqvist, K.-I.; Forsen, S. *J. Phys. Chem.* **1965**, *69*, 4062−4071.
(61) Casarini, D.; Lunazzi, L.; Macciantelli, D. *J. Chem. Soc., Perkin Trans. 2* **1985**, 1839−1844.
(62) Benassi, R.; Folli, U.; Schenetti, L.; Taddei, F. *J. Chem. Soc., Perkin Trans. 2* **1987**, 961−968.
(63) Abraham, R. J.; Siverns, T. M. *Tetrahedron* **1972**, *28*, 3015−3023.
(64) Han, I.; Kim, C. K.; Jung, H. J.; Lee, I. *Theor. Chim. Acta* **1996**, *93*, 199−210.
(65) Dahlqvist, K.-I.; Forsen, S. *J. Phys. Chem.* **1965**, *69*, 1760−1761.
(66) Kotzian, M.; Kreiter, C. G.; Michael, G.; Ozkar, S. *Chem. Ber.* **1983**, *116*, 3637−3658.
(67) Naorem, H.; Kishore, N.; Suri, S. K. *Can. J. Chem.* **1989**, *67*, 648−650.
(68) Muhandiram, D. R.; McClung, R. E. D. *J. Magn. Reson.* **1987**, *71*, 187−192.
(69) Frisch, M. J.; Truck, G. W.; Schlegel, H. B.; Gill, P. M. W.; Johnson, B. G.; Robb, M. A.; Cheeseman, J. R.; Keith, T. A.; Petersen, G.; Montgomery, J. A.; Raghavachari, K.; Al-Laham, M. A.; Zakrzewski, V. G.; Ortiz, J. V.; Forseman, J. B.; Cioslowski, J.; Stefanov, B.; Nanayakkara, A.; Challacombe, M.; Peng, C. Y.; Ayala, P. Y.; Chen, W.; Wong, M. W.; Andres, J. L.; Replogle, E. S.; Gomperts, R.; Martin, R. L.; Fox, D. J.; Binkley, J. S.; Defrees, D. J.; Baker, J.; Stewart, J. P.; Head-Gordon, M. W.; Gonzalez, C.; Pople, J. A. *Gaussian 94*; Gaussian, Inc.: Pittsburgh, PA, 1995.
(70) *CRC Handbook of Chemistry and Physics*; 49th ed.;The Chemical Rubber Co.: Cleveland, 1968; pp E-58−E-61.